Multi-scale Optical Flow Including Normalized Mutual Information for Planar Deformable Lung Motion Estimation from 4D CT

Mohammadreza Negahdar and Amir A. Amini, *IEEE Fellow*

Abstract—A novel energy function for computing planar optical flow from X-ray CT images was presented and reported in detail in [1]. The technique combines four terms: brightness constancy, gradient constancy, continuity equation based on mass conservation, and discontinuity-preserving spatio-temporal smoothness. Both qualitative and quantitative evaluation of the proposed method demonstrated that the method results in significantly better angular errors than previous well-known techniques for optical flow estimation. A multi-scale approach to motion field computation based on this framework is presented in this paper. The proposed approach significantly speeds up the calculations, realizing computational savings. Additionally, an approach to determination of optimum values of scalar weights in the energy function is herein proposed. Normalized mutual information measured between the first image warped with the estimated motion and the second image is used to determine the optimum value for weighting parameters.

I. INTRODUCTION

Deformable image registration has received much attention in the literature [3-6]. Medical image registration may involve registration of longitudinally acquired images to elucidate anatomical changes occurring due to disease progression, or from result of therapy. However, it can also be used to track temporally acquired data such as 4D lung images acquired with X-ray computed tomography (CT). Registration of thoracic CT images is of particular interest to the medical community since it can provide a mechanism to determine the respiratory motion while the compressible nature of lung tissue which results in varying voxel intensities makes accurate deformable registration of 4D CT thoracic image data difficult to achieve. The ability to track the motion of lung using 4D CT imaging may give more information on regional lung function, assessment of disease severity, and inform better about prognosis. With this as the driving goal, we arrive at a new variational formulation for optical flow and compare its performance to that of well-known optical flow methods.

The basic assumption in standard optical flow estimation is grey value constancy assumption which is not particularly applicable to lung motion estimation. In this work, we include gradient constancy, mass conservation, as well as spatio-temporal smoothness to more accurately model and estimate motion of the lung. For comparing the accuracy of the proposed method, we employ the average angular error (AAE) and weighted angular error (WAE) between the computed motion fields and ground truth motion known at number of 2-D landmark points within the lung volume.

It should be noted that in the past a number of papers have proposed techniques for non-rigid lung motion estimation [2, 7-9]. These have for the most part been based on free-form deformation paradigm. In comparison to such techniques, our optical flow framework has the advantage that it provides the possibility to enforce physical constraints on the flow field. Although the theoretical basis of our present approach was previously described in [1], the primary contributions of the present paper are a fast implementation through use of multiple computational scales as well as determination of optimum parameters for the energy function through use of normalized mutual information.

II. METHOD

As outlined in [1], in order to derive a variational formulation for our optical flow method, below, we list the constraints of interest.

(I) Ideally, the gray value of a pixel should not change after displacement:

$$I(X + W) = I(X) \qquad (1)$$

In (1) I is the image intensity as a function of space and time, $X := (x, y, t)^T$, and $W := (u, v, 1)^T$ is the displacement vector field between two subsequent images. This is a nonlinear equation in u and v. Its linearized version yields the well-known optical flow constraint [10]:

$$I_x u + I_y v + I_t = 0 \qquad (2)$$

known as the optical flow equation, first described in [10].

(II) In the case of thoracic CT images, tissue densities and consequently voxel intensities, change from one image to the next due to breathing. Despite local tissue density fluctuations caused by perfusion, we assume the imaged intensities follow a conservation principle in analogy to mass conservation in fluid flow. In fact, one can show that if it can be assumed that the Hounsfield unit is proportional to density then the two conservation principles are equivalent. Application of the conservation principle to a temporally varying image yields:

$$\nabla . (IV) + I_t = 0 \;\Rightarrow\; \nabla I . (V) + I(\nabla . V) + I_t = 0 \qquad (3)$$

$$I_x u + I_y v + I u_x + I v_y + I_t = 0 \qquad (4)$$

where $V = (u, v)$ is the velocity field. Equation (4) is a more general constraint for deformable object motion in comparison to the classic Horn-Schunck optical flow constraint equation shown in (2).

(III) In order to allow variations in the grey value and to help determine the displacement vector by a criterion that favors matching moving edges, a constraint based on image gradients is also incorporated:

$$\nabla I(X + W) = \nabla I(X) \tag{5}$$

(IV) Finally, in order to regularize the solution, spatio-temporal smoothness of the flow field is adopted:

$$|\nabla_3 u|^2 + |\nabla_3 v|^2 \tag{6}$$

where $\nabla_3 := (\partial_x, \partial_y, \partial_t)^T$. Therefore, the energy functional that penalizes deviations from these model assumptions is measured by:

$$E(u,v) = E_D + \alpha E_S = \int_\Omega \psi[|I(X+W) - I(X) + \beta(I\nabla.V)|^2 + \gamma|\nabla I(X+W) - \nabla I(X)|^2 dX + \int_\Omega \alpha \psi|\nabla_3 u|^2 + |\nabla_3 v|^2 dX \tag{7}$$

where β can only be zero or one: zero when the object is incompressible and one when the object is compressible.

$I_x := \frac{\partial}{\partial x} I(X + W)$, $\quad I_y := \frac{\partial}{\partial y} I(X + W)$, $\quad I_\phi := I(X + W) - I(X)$,

$I_{xx} := \frac{\partial^2}{\partial x^2} I(X + W)$, $\quad I_{yy} := \frac{\partial^2}{\partial y^2} I(X + W)$, $\quad I_{xy} := \frac{\partial^2}{\partial x \partial y} I(X + W)$,

$I_{x\phi} := \frac{\partial}{\partial x} I(X + W) - \frac{\partial}{\partial x} I(X)$, $\quad I_{y\phi} := \frac{\partial}{\partial y} I(X + W) - \frac{\partial}{\partial y} I(X)$.

The function $\psi(s^2) = \sqrt{s^2 + \varepsilon^2}$ is a modified L_1 norm which is convex and offers advantages in the minimization process namely robustness to outliers. Since ε is only utilized for numerical reasons, it can be set to a fixed value (we chose 0.001).

A minimizer of $E(u, v)$ must fulfill the Euler-Lagrange equations:

$$\begin{cases} E_u - \frac{\partial}{\partial x} E_{u_x} - \frac{\partial}{\partial y} E_{u_y} - \frac{\partial}{\partial t} E_{u_t} = 0 \\ E_v - \frac{\partial}{\partial x} E_{v_x} - \frac{\partial}{\partial y} E_{v_y} - \frac{\partial}{\partial t} E_{v_t} = 0 \end{cases} \tag{8}$$

Therefore

$$\begin{cases} \psi'\left[I_\phi^2 + (\beta(I\nabla.V))^2 + 2I_\phi(\beta(I\nabla.V)) + \gamma(I_{x\phi}^2 + I_{y\phi}^2)\right] + \\ (I_x I_\phi + I_x I_\phi(\beta(I\nabla.V)) + \gamma(I_{xx} I_{x\phi} + I_{xy} I_{y\phi}) - \beta(I\nabla.V)(1 + I_\phi)) - \\ \qquad \alpha \, div(\psi'[|\nabla_3 u|^2 + |\nabla_3 v|^2]\nabla_3 u) = 0 \\ \\ \psi'\left[I_\phi^2 + (\beta(I\nabla.V))^2 + 2I_\phi(\beta(I\nabla.V)) + \gamma(I_{x\phi}^2 + I_{y\phi}^2)\right] + \\ (I_y I_\phi + I_y I_\phi(\beta(I\nabla.V)) + \gamma(I_{xy} I_{x\phi} + I_{yy} I_{y\phi}) - \beta(I\nabla.V)(1 + I_\phi)) - \\ \qquad \alpha \, div(\psi'[|\nabla_3 u|^2 + |\nabla_3 v|^2]\nabla_3 v) = 0 \end{cases} \tag{9}$$

with the iteration variable W^k instead of W, W^{k+1} will be the solution of;

$$\begin{cases} \psi'\left[I_\phi^{k+1^2} + (\beta(I^k\nabla.(u^{k+1}, v^{k+1})))^2 + 2I_\phi^{k+1}(\beta(I^k\nabla.(u^{k+1}, v^{k+1}))) + \gamma(I_{x\phi}^{k+1^2} + I_{y\phi}^{k+1^2})\right] + \\ (I_x^k I_\phi^{k+1} + I_x^k I_\phi^{k+1}(\beta(I^k\nabla.(u^{k+1}, v^{k+1}))) + \gamma(I_{xx}^k I_{x\phi}^{k+1} + I_{xy}^k I_{y\phi}^{k+1}) - \beta(I^k\nabla.(u^{k+1}, v^{k+1}))(1 + I_\phi^{k+1})) - \\ \qquad \alpha \, div(\psi'[|\nabla_3 u^{k+1}|^2 + |\nabla_3 v^{k+1}|^2]\nabla_3 u^{k+1}) = 0 \\ \\ \psi'\left[I_\phi^{k+1^2} + (\beta(I^k\nabla.(u^{k+1}, v^{k+1})))^2 + 2I_\phi^{k+1}(\beta(I^k\nabla.(u^{k+1}, v^{k+1}))) + \gamma(I_{x\phi}^{k+1^2} + I_{y\phi}^{k+1^2})\right] + \\ (I_y^k I_\phi^{k+1} + I_y^k I_\phi^{k+1}(\beta(I^k\nabla.(u^{k+1}, v^{k+1}))) + \gamma(I_{xy}^k I_{x\phi}^{k+1} + I_{yy}^k I_{y\phi}^{k+1}) - \beta(I^k\nabla.(u^{k+1}, v^{k+1}))(1 + I_\phi^{k+1})) - \\ \qquad \alpha \, div(\psi'[|\nabla_3 u^{k+1}|^2 + |\nabla_3 v^{k+1}|^2]\nabla_3 v^{k+1}) = 0 \end{cases} \tag{10}$$

To remove the nonlinearity in I_*^{k+1}, first order Taylor expansion yields

$$I_\phi^{k+1} \approx I_\phi^k + I_x^k du^k + I_y^k dv^k$$
$$I_{x\phi}^{k+1} \approx I_{x\phi}^k + I_{xx}^k du^k + I_{xy}^k dv^k$$
$$I_{y\phi}^{k+1} \approx I_{y\phi}^k + I_{xy}^k du^k + I_{yy}^k dv^k$$

where $u^{k+1} = u^k + du^k$ & $v^{k+1} = v^k + dv^k$.

Introducing an abbreviation for the robustness factor ψ'_{Data} and the diffusivity ψ'_{Smooth},

$$(\psi'_{data})^k := \psi'\left[(I_\phi^k + I_x^k du^k + I_y^k dv^k)^2 + (\beta(I^k\nabla.(u^k + du^k, v^k + dv^k2 + 2I\phi k + Ixk du k + Iyk dvk\beta I k\nabla.uk + duk, vk + dvk + \gamma Ix\phi k + Ixxk duk + Ixykdvk2 + Iy\phi k + Ixykdu k + Iyykdvk2 \tag{11}$$

$$(\psi'_{Smooth})^k := \psi'\left[|\nabla_3(u^k + du^k)|^2 + |\nabla_3(v^k + dv^k)|^2\right] \tag{12}$$

As the only remaining nonlinearity is due to ψ', and ψ has been chosen to be a convex function, the remaining optimization problem is a convex problem; i.e., there exists a unique minimum. To remove the remaining nonlinearity in ψ', a second, inner fixed point iteration loop is applied. Let l denote the iteration index for this inner loop. The fixed point variables $du^{k,l}$ and $dv^{k,l}$ are both initialized with 0. Therefore, the linear system of equations in $du^{k,l+1}$ and $dv^{k,l+1}$:

$$(\psi'_{Data})^{k,l}\left(I_x^k(I_\phi^k + I_x^k du^{k,l+1} + I_y^k dv^{k,l+1})\left(1\right.\right.$$
$$+ \beta\left(I^k\nabla.(u^k + du^{k,l+1}, v^k + dv^{k,l+1})\right)\right)$$
$$+ \gamma\left(I_{xx}^k(I_{x\phi}^k + I_{xx}^k du^{k,l+1} + I_{xy}^k dv^{k,l+1})\right.$$
$$+ I_{xy}^k(I_{y\phi}^k + I_{xy}^k du^{k,l+1} + I_{yy}^k dv^{k,l+1})\right)$$
$$- \beta\left(I^k\nabla.(u^k + du^{k,l+1}, v^k + dv^{k,l+1})\right)\left(1\right.$$
$$\left.\left.+ (I_\phi^k + I_x^k du^{k,l+1} + I_y^k dv^{k,l+1})\right)\right)$$
$$- \alpha \, div((\psi'_{Smooth})^{k,l}[\nabla_3(u^k + du^{k,l+1})]) = 0 \tag{13-1}$$

$$(\psi'_{Data})^{k,l}\left(I_y^k(I_\phi^k + I_x^k du^{k,l+1} + I_y^k dv^{k,l+1})\left(1\right.\right.$$
$$+ \beta\left(I^k\nabla.(u^k + du^{k,l+1}, v^k + dv^{k,l+1})\right)\right)$$
$$+ \gamma\left(I_{xy}^k(I_{x\phi}^k + I_{xx}^k du^{k,l+1} + I_{xy}^k dv^{k,l+1})\right.$$
$$+ I_{yy}^k(I_{y\phi}^k + I_{xy}^k du^{k,l+1} + I_{yy}^k dv^{k,l+1})\right)$$
$$- \beta\left(I^k\nabla.(u^k + du^{k,l+1}, v^k + dv^{k,l+1})\right)\left(1\right.$$
$$\left.\left.+ (I_\phi^k + I_x^k du^{k,l+1} + I_y^k dv^{k,l+1})\right)\right)$$
$$- \alpha \, div((\psi'_{Smooth})^{k,l}[\nabla_3(v^k + dv^{k,l+1})]) = 0 \tag{13-2}$$

Discretization yields a linear system of equations, which can be solved by Successive Over Relaxation (SOR). Let m denote the iteration index for the SOR iterations, then the iteration scheme for solving the linear system is:

$$du_i^{k,l,m+1} = (1-\omega)du_i^{k,l,m} + \omega \frac{\sum_{j\in N^-(i)}(\psi'_{Smooth})_{i\sim j}^{k,l}(u_j^k + du_j^{k,l,m+1}) + \sum_{j\in N^+(i)}(\psi'_{Smooth})_{i\sim j}^{k,l}(u_j^k + du_j^{k,l,m}) - \sum_{j\in N^-(i)\cup N^+(i)}(\psi'_{Smooth})_{i\sim j}^{k,l}u_j^k}{\sum_{j\in N^-(i)\cup N^+(i)}(\psi'_{Smooth})_{i\sim j}^{k,l} + \frac{(\psi'_{Data})_i^{k,l}}{\alpha}\left(((I_x)_i^k)^2 + \left((I_{xy})_i^k\right)^2 + ((I_{xx})_i^k)^2 + (I)_i^k(I_x)_i^k\right)}$$

$$-\omega\frac{\frac{(\psi'_{Data})_i^{k,l}}{\alpha}\left(((1+B)I_x)_i^k\left((I_y)_i^k dv_i^{k,l,m} + (I_\phi)_i^k\right) + \gamma\left((I_{xx})_i^k\left((I_y)_i^k dv_i^{k,l,m} + (I_{x\phi})_i^k\right) + (I_{xy})_i^k\left((I_{yy})_i^k dv_i^{k,l,m} + (I_{y\phi})_i^k\right)\right) + (BI)_i^k\left((I_y)_i^k dv_i^{k,l,m} - (I_\phi)_i^k - 1\right)\right)}{\sum_{j\in N^-(i)\cup N^+(i)}(\psi'_{Smooth})_{i\sim j}^{k,l} + \frac{(\psi'_{Data})_i^{k,l}}{\alpha}\left(((I_x)_i^k)^2 + \left((I_{xy})_i^k\right)^2 + ((I_{xx})_i^k)^2 + (I)_i^k(I_x)_i^k\right)}$$

$$(14\text{-}1)$$

$$dv_i^{k,l,m+1} = (1-\omega)dv_i^{k,l,m} + \omega \frac{\sum_{j\in N^-(i)}(\psi'_{Smooth})_{i\sim j}^{k,l}(v_j^k + dv_j^{k,l,m+1}) + \sum_{j\in N^+(i)}(\psi'_{Smooth})_{i\sim j}^{k,l}(v_j^k + dv_j^{k,l,m}) - \sum_{j\in N^-(i)\cup N^+(i)}(\psi'_{Smooth})_{i\sim j}^{k,l}v_j^k}{\sum_{j\in N^-(i)\cup N^+(i)}(\psi'_{Smooth})_{i\sim j}^{k,l} + \frac{(\psi'_{Data})_i^{k,l}}{\alpha}\left(\left((I_y)_i^k\right)^2 + \left((I_{xy})_i^k\right)^2 + \left((I_{yy})_i^k\right)^2 + (I)_i^k(I_y)_i^k\right)}$$

$$-\omega\frac{\frac{(\psi'_{Data})_i^{k,l}}{\alpha}\left(((1+B)I_y)_i^k\left((I_x)_i^k du_i^{k,l,m} + (I_\phi)_i^k\right) + \gamma\left((I_{xy})_i^k\left((I_{xx})_i^k du_i^{k,l,m} + (I_{x\phi})_i^k\right) + (I_{yy})_i^k\left((I_y)_i^k du_i^{k,l,m} + (I_{y\phi})_i^k\right)\right) + (BI)_i^k\left((I_x)_i^k du_i^{k,l,m} - (I_\phi)_i^k - 1\right)\right)}{\sum_{j\in N^-(i)\cup N^+(i)}(\psi'_{Smooth})_{i\sim j}^{k,l} + \frac{(\psi'_{Data})_i^{k,l}}{\alpha}\left(\left((I_y)_i^k\right)^2 + \left((I_{xy})_i^k\right)^2 + \left((I_{yy})_i^k\right)^2 + (I)_i^k(I_y)_i^k\right)}$$

$$(14\text{-}2)$$

where $B = \beta\left(I^k \nabla.(u^k + du^{k,l}, v^k + dv^{k,l})\right)$.

It can be shown that this algorithm will be simplified to the method proposed by Brox et al. [11] when $\beta = 0$, while it would result in the modified version of the Wildes method [12] with $\gamma = 0$. In the simplest form, with both $\beta = 0$ and $\gamma = 0$, the proposed method simplifies to Horn-Schunck method [10], though with spatio-temporal smoothness.

Since the proposed method converges to the estimated motion in an iterative form, a multi-scale framework was used to speed up the calculations realizing significant computational savings. A multiresolution strategy helps to improve computational efficiency and to avoid local minima [5]. Both frames are first downsampled by a factor of 2 in each dimension in order to reduce the computational time. The downsampled images are then registered in the multiresolution framework. Once the registration is completed, the warped image is upsampled so that it has the same size as the reference image.

If necessary, the number of scales in the multiresolution approach just described could be further increased with the warped image propagated to the next finer level and used as a starting transformation for that level.

While the proposed method leads toward an accurate motion estimation, the number of weighting factors- that is α, γ, and l- and their various combinations is a significant challenge. To find the optimum weights, normalized mutual information (NMI)[13] has been used as a similarity measure between the first frame warped with the calculated motion field and the second frame. NMI is essentially used here as the yardstick to compare the accuracy of the estimated motion for different weighting factors [13-16]. Fig. 1 shows a similarity calculation between the first warped frame and the second frame for five different alpha, that is from 10 to 50 which increments by 10, five different gamma, that is from 50 to 210 which increments by 40, for $l = 5, 6$.

III. RESULTS

The proposed method has been applied on some well-known images where the scenario of mass conservation does or does not hold. The related results have been reported in detail in [1]. For both qualitative and quantitative evaluation of the proposed method, Popi-model data-set of lung deformation has been used [17]. It is a pixel-based and point-validated breathing thorax model which is used to validate the results of our method. The anonymized respiration-correlated 4D CT image consists of 10 3D CT images sampling the entire respiratory cycle. Each 3D image volume is made up of 141 axial slices with a slice thickness of 2mm. Each slice is a 2D image with size 512x512 with an isotropic in-plane resolution of 0.97 mm. Landmarks are defined by experts
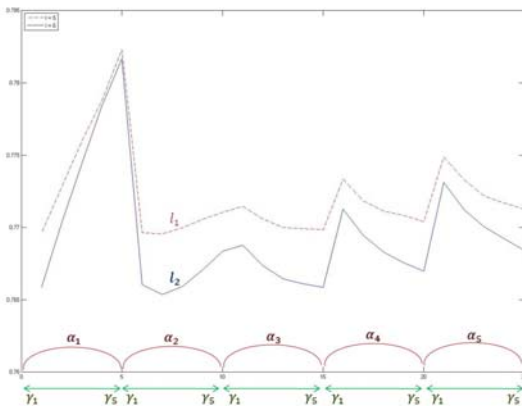

Figure 1: Similarity calculation between the first warped image and the second image. This Graph shows similarity calculation in terms of five gamma ($\gamma_1 \sim \gamma_5$) and five alpha ($\alpha_1 \sim \alpha_5$) values for two different number of levels (l_1, l_2).
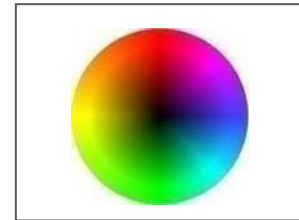

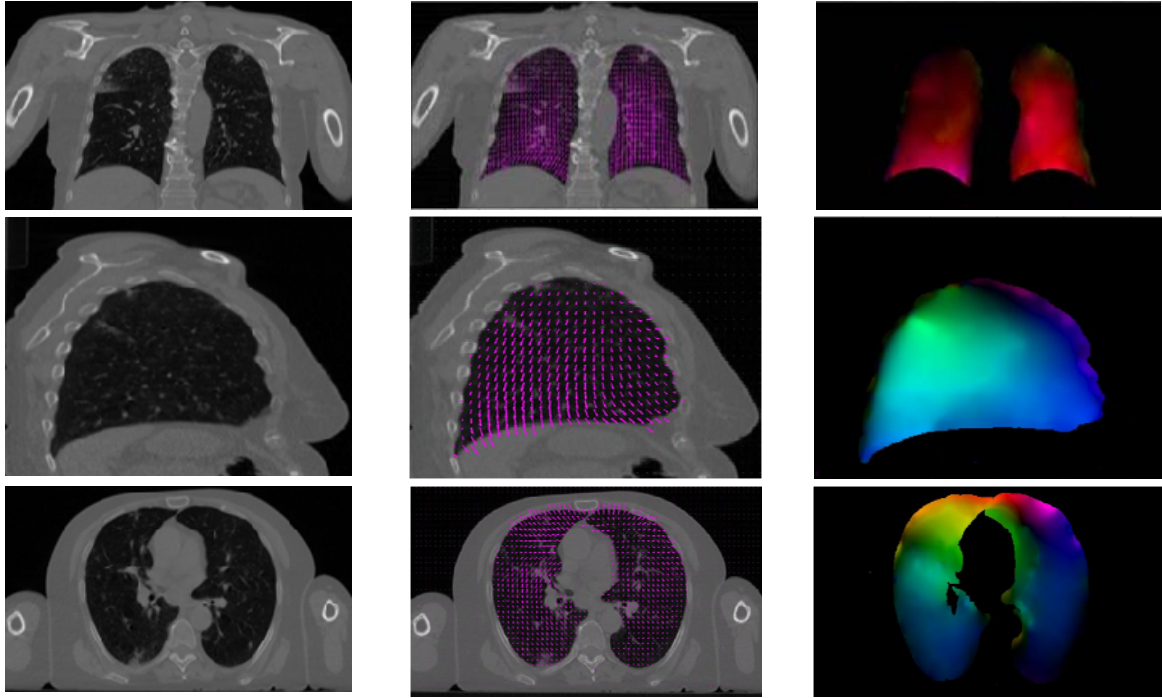Figure 2: Color wheel for encoding motion vectors.

Figure 3: Top row: coronal, and bottom row: transversal planes of the lung. From left to right: (a) First frame. (b) Calculated vector field superimposed on the first frame with $\alpha = 50, \gamma = 150, \beta = 1$. Note that these parameters were also used in the 6th row of table 1 labeled "Proposed Method". (c) Color coded diagram of the related vector filed (based on Figure 1).

in all of the 3D CT image volumes that make up the 4D CT data. Since the implemented algorithms work on planar images in time, the only landmarks that were used for validation of our technique were those that have planar motion in subsequent frames. Fig. 3 shows calculated vector field in all three anatomical orientations. The average computational time to arrive at these results were 38 seconds within a multi-scale framework on a Dell 5160 machine with a quad-core Xeon 3.00 GHz processor. As shown in the color wheel (Fig. 2) used to visualize flow fields in this paper, smaller vectors are darker while the color indicates direction of movement. Whereas images in Fig. 3 give a good visual impression of the results, the fact that ground truth motion is available for the landmark points also offers the possibility to have a quantitative measure of the quality of the estimated optical flow. Such a quantitative measure to assess and compare the performance of the method has been introduced with the so-called average angular error (AAE) in [18] and weighted angular error (WAE) in [2]. Assume the computed motion field $V_c = (u_c, v_c)$ and the ground truth vector field $V_g = (u_g, v_g)$, the AAE of the calculated flow field can be computed by

$$AAE := \frac{1}{n} \sum_{i=1}^{n} arccos \left(\frac{(u_c)_i (u_g)_i + (v_c)_i (v_g)_i + 1}{\sqrt{((u_c)_i^2 + (v_c)_i^2 + 1)((u_g)_i^2 + (v_g)_i^2 + 1)}} \right) \quad (15)$$

where n denotes the total number of the landmark points. This expression not only measures the spatial angular error between the estimated flow vector and the correct vector, but also the differences in the magnitude of both vectors, since it evaluates the angular error of the spatio-temporal vector $(u_c, v_c, 1)$.

In the metric shown in (16), the individual angle deviations have been weighed by the magnitude of the landmark displacement vector; normalized by the sum of magnitude of all ground truth vectors. The reason for this is to emphasize angle deviation of points which have large displacements, and similarly to de-emphasize the angle deviation of points which have a smaller displacement.

$$\frac{1}{\sum |V_g|} \sum \left(|V_g| . \cos^{-1} \frac{V_g . V_c}{|V_g||V_c|} \right) \quad (16)$$

Table-1 reports these results in comparison with the well-known optical flow methods which were reported in [2].

IV. CONCLUSIONS

In conclusion, we have proposed a multi-scale implementation of an optical flow framework based on a mass conservation and image gradient constancy, previously derived and reported in [1]. In addition to multi-scale implementation, a novelty of the approach

Table 1: Quantitative evaluation and comparison of the already implemented methods [2] and the proposed method. AAE and WAE stand for *average angular error* and *weighted angular error*, respectively. Mean errors are shown with (standard deviation) for each case.

Method	AAE	WAE
Horn-Schunck(Global) [10]	92.65° (9.3°)	91.4° (10.6°)
Lucas-Kanade(Local) [19]	92.62° (11.5°)	92.22° (12.8°)
CLG(Local-Global) [20]	89.88° (9°)	89.7° (9.8°)
Proposed Method simplified to Brox et al. [11]	28.93° (3.7°)	36.1°(3.9°)
Proposed Method simplified to Wildes [12]	28.22° (3.5°)	35.89° (3.8°)
Proposed Method	26.98° (3.1°)	34.2° (3.2°)

proposed in this paper is determination of the optimum values of scalar weights in the energy function based on the normalized mutual information similarity metric measured between the first image warped with the estimated motion and the second image. The proposed optical flow framework provides the possibility to enforce physical constraints on the velocity field to handle the difficulties inherent in the thoracic CT image registration problem. As shown in table 1, the proposed method performs well with respect to both AAE and WAE, meaning that amongst the optical flow methods which were evaluated, we expect better estimation of the lung's planar motion using the proposed algorithm. This motivates the use of physical constraints which were utilized in our numerical implementation

Nonetheless, it should be noted that the presented method was only evaluated for planar motion estimation whereas most deformable motions including lung's motion are 3D. This will be challenging since the computational requirements in 3D are expected to increase substantially over 2D. This is direction for future work.

REFERENCES

[1] M. Negahdar, and A. A. Amini, "Planar deformable motion estimation incorporating mass conservation and image gradient constancy," in ISBI, Chicago, IL, USA, pp. 536-540, 2011.

[2] M. Negahdar, and A. A. Amini, "Tracking planar lung motion in 4D CT with optical flow: validations and comparison of global, local, and local-global methods," in SPIE, San Diego, CA, USA pp. 762623, 2010.

[3] D. Sarrut, "Deformable registration for image-guided radiation therapy," *Zeitschrift fur Medizinische Physik,* vol. 16, no. 4, pp. 285-297, 2006.

[4] K. K. Brock, M. B. Sharpe, L. A. Dawson, *et al.*, "Accuracy of finite element model-based multi-organ deformable image registration," *Medical Physics,* vol. 32, no. 6, pp. 1647-1659, 2005.

[5] Y. Yin, E. A. Hoffman, and C.-L. Lin, "Local tissue-weight-based nonrigid registration of lung images with application to regional ventilation," in SPIE Conf. Medical Imaging, pp. 72620C, 2009.

[6] E. Castillo, Y. Zhang, R. Tapia, *et al.*, "Compressible image registration for thoracic computed tomography images," *Journal of Medical and Biological Engineering,* vol. 29, no. 5, pp. 222-233, 2009.

[7] T. Guerrero, G.Zhang, T. Huang, *et al.*, "Intrathoracic tumour motion estimation from CT imaging using the 3D optical flow method," *Physics in Medicine and Biology,* vol. 49, pp. 4147-4161, 2004.

[8] F. Li, C.-W. Chen, E. A. Hoffman, *et al.*, "Evaluation and application of 3D lung warping and registration model using HRCT images," in SPIE Conf. Medical Imaging, pp. 234-243, 2001.

[9] J. M. Reinhardt, G. E. Christensen, E. A. Hoffman, *et al.*, "Registration-derived estimates of local lung expansion as surrogates for regional ventilation," *Lecture Notes in Computer Science*, Kerkrade, The Netherlands: Springer Berlin/Heidelberg, 2007.

[10] B. K. P. Horn and B. G. Schunck, "Determining optical flow," *Artificial Intelligence,* vol. 17, pp. 185-203, 1981.

[11] T. Brox, A. Bruhn, N. Papenberg, *et al.*, "High accuracy optical flow estimation based on a theory of warping," in ECCV, Czech Republic, pp. 25-36, 2004.

[12] R. P. Wildes, M. J. Amabile, A.-M. Lanzillotto, *et al.*, "Recovering estimates of fluid flow from image sequence data," *Computer Vision and Image Understanding,* vol. 80, no. 2, pp. 246-266, 2000.

[13] C. Studholme, D. L. G. Hill, and D. J. Hawkes, "An overlap invariant entropy measure of 3D medical image alignment," *Pattern Recognition,* vol. 32, no. 1, pp. 71-86, 1999.

[14] C. Hua-Mei, P. K. Varshney, and M. K. Arora, "Performance of mutual information similarity measure for registration of multitemporal remote sensing images," *IEEE Transactions on Geoscience and Remote Sensing,* vol. 41, no. 11, pp. 2445-2454, 2003.

[15] L. Papp, M. Zuhayra, E. Henze *et al.*, "Extended Normalized Mutual Information for Lung SPECT - CT Registration," in 3rd International Conference on Bioinformatics and Biomedical Engineering , 2009. ICBBE 2009., Beijing, China, pp. 1-3, 2009.

[16] R. Chandrashekara, R. H. Mohiaddin, and D. Rueckert, "Analysis of 3-D myocardial motion in tagged MR images using nonrigid image registration," *IEEE Transactions on Medical Imaging,* vol. 23, no. 10, pp. 1245-1250, 2004.

[17] J. Vandemeulebroucke, D. Sarrut, and P. Clarysse, "The POPI-model, a point-validated pixel-based breathing thorax model," in International Conference on the Use of Computers in Radiation Therapy (ICCR), Toronto, Canada, 2007.

[18] J. L. Barron, D. J. Fleet, and S. S. Beauchemin, "Performance of optical flow techniques," *International Journal of Computer Vision (IJCV),* vol. 12, no. 1, pp. 43-77, February, 1994.

[19] B. D. Lucas, and T. Kanade, "An iterative image registration technique with an application to stereo vision," in Proceedings of DARPA Image Understanding workshop, pp. 121-130, 1981.

[20] J. Weickert, A. Bruhn, and C. Schnorr, "Lucas/Kanade meets Horn/Schunck: combining local and global optic flow methods," *International Journal of Computer Vision,* vol. 61, no. 3, pp. 211-231, 2005.